Molecular dynamics studies of entangled polymer chains

Bulacu, Monica Iulia

Chapter 5

Glass transition

I do not understand the subject any better, but I am now confused at a much higher level.

Enrico Fermi

This chapter presents computation results obtained from extensive coarse-grained molecular-dynamics simulations of amorphous ensembles of polymer chains at constant density. In our polymer model, we use bending and torsion potentials acting along the polymer backbone to control the chain stiffness. The static and dynamic properties of the polymer bulk have been analyzed over a large temperature interval in search for the onset of the glass transition. The glass transition temperatures $T_{\rm g}$, for different types of chain stiffness, have been determined from the dependence of the self-diffusion coefficient D on the temperature T as the limiting value where the diffusion vanishes. Increasing the chain stiffness induces an increase of the glass transition temperature. The $T_{\rm g}$ values estimated from diffusion are confirmed by analyzing the relaxation times of the autocorrelation functions for the torsion angle and for the end-to-end vector. The dependence of the diffusion coefficient D on the chain length N is strongly affected by temperature for chains with bending and torsion stiffness. For systems with relatively short chains ($N \leq 50$), the exponent ν from $D \propto N^{-\nu}$ increases from the value $\nu \approx 1$ expected in the Rouse regime to $\nu \approx 2$ as the temperature is lowered towards $T_{\rm g}$.

[0]Based on *Molecular-dynamics simulation study of the glass transition in amorphous polymers with controlled chain stiffness*, Monica Bulacu and Erik Van der Giessen, Phys. Rev. E, 76, 011807 (2007).

5.1 Introduction

The glass transition temperature T_g is one of the most important attributes of amorphous polymers for two main reasons. First, T_g characterizes the local chain dynamics and represents an intrinsic signature of the internal structure. Second, below this temperature, in the glassy state, amorphous polymers find countless technical applications. However, the complex process of the glass transition is still not yet completely understood, motivating Philip W. Anderson (Nobel Laureate in Physics) to state in 1995: "the deepest and most interesting unsolved problem in solid state theory is probably the theory of glass and the glass transition temperature. This could be the next breakthrough in the coming decade [...]. Whether it will help make better glass is questionable" (Anderson 1995).

Computer simulations—here we refer in particular to molecular-dynamics (MD) methods— of polymeric systems at low temperatures can help in the development and validation of a theory of glass transition by allowing a large palette of virtual 'experiments' in which different factors can be investigated separately. A significant advantage over laboratory experiments is that MD simulations make possible a much more detailed analysis of both material structure and local dynamics. However, the time range accessible to computer simulations is, inevitably, very short and the number of direct experimental techniques that can cover it is very reduced. This limits the set of observable properties that can be monitored both by experiment and by computer methods and obtaining comparable T_g values remains difficult.

Due to this insurmountable time limitation, only relatively high temperatures are feasible in MD simulations. This frustrates comparison between simulation results and the predictions of early T_g theories involving low critical temperatures (Gibbs and DiMarzio 1958, Turnbull and Cohen 1961). Fortunately, more recent theories (Götze and Sjögren 1992) deal with concepts at smaller time scales and higher critical temperatures where computer simulations can indeed be a powerful test. We refer the interested reader to a few extensive review articles on the theoretical concepts underlying T_g and their correspondence with simulation and experimental results (Binder et al. 2003, Kob 1999, Ediger et al. 1996).

Majority of MD simulation studies have tried to identify T_g by monitoring changes of certain macroscopic or microscopic properties during cooling. Early works, using a united-atom polyethylene model (Rigby and Roe 1987, Takeuchi and Okazaki 1990, Takeuchi and Roe 1991, Roe 1994), have investigated the static and dynamic properties of polymer chain ensembles and the most important signs indicating glass transition were a distinct kink in the temperature dependence of the specific volume and a continuous change in the time dependence of the chain mean-square displacements at decreasing temperature values. Using the same polyethylene model, very similar values

of T_{g} have been obtained from non-equilibrium MD simulations of stress relaxation in polymer melts (Gao and Weiner 1992, Weiner and Gao 1994).

More recently, other studies have predicted the glass transition temperature for specific polymer species by including more chemical detail in the simulations (Tsige and Taylor 2002, Lyulin et al. 2003, Han et al. 1994, Yu et al. 2001).

Polymers with very different chemical configurations go through glass transition, thus rendering it a universal phenomenon. Therefore, it is appealing to study the glass transition using a simple and elegant coarse-grained polymer model that is safe from chemical details and is computationally efficient. The well-known coarse-grained model introduced by Kremer and Grest (1990) is very convenient, giving access to long simulation times, and it has already been used with success in many polymer dynamics studies. Here, we will also use the Kremer-Grest model, but augmented with bending and torsion potentials to control the chain stiffness, and we systematically investigate the effect of temperature on polymer melt behavior.

In the Kremer-Grest model, each polymer chain is represented by a sequence of beads connected by un-harmonic springs while all beads in the system interact via a purely repulsive Lennard-Jones (LJ) potential. The dynamics of a polymer melt is determined by the entanglement between the chains of the ensemble, and this has direct implications on the physical properties of the system, including phase transitions and T_{g}. The authors of the model suggested themselves that the temperature at which all the simulations were performed, $T = 1.0\varepsilon/k_{\mathrm{B}}$, is "at least a factor of 2 above T_{g}."

The most cited papers when referring to the glass transition temperature T_{g} of systems based on the Kremer-Grest model are Baljon and Robbins (1996, 1997). These assign the glass transition to "just below $0.6\varepsilon/k_{\mathrm{B}}$" by looking at the shear response in thin polymer films. However, these simulations are conducted at constant null pressure and the LJ potential includes an attractive part. The T_{g} value was also estimated for polymer bulks (at constant pressure and volume) (Bennemann et al. 1998) and for random polymer network with cross-links (Stevens 2001) by simulations that include as well an attractive part of the LJ interaction.

A recent temperature study using the Kremer-Grest (repulsive LJ) model has been performed by Yamamoto and Onuki (2002) which by simulating supercooled polymer melts in shear flow have not seen any characteristics of the glassy state even for $T = 0.2\varepsilon/k_{\mathrm{B}}$.

It is very difficult to compare all these values of T_{g} because they have been computed for bulks, films, or networks and the simulations were run under different conditions (constant-pressure versus constant-volume), with different values of the LJ cutoff distance (including or not attractive interactions) and, especially, involving various polymer chain lengths or densities. On the other hand, a methodic analysis of the temperature effects in polymer bulks for finding clear evidence of glass transition in polymer

bulks was still needed. We focus our study on polymer melts simulated at constant volume using purely repulsive LJ interactions. The first aim of the current work is therefore to systematically cover this middle ground that remained to some extent insufficiently studied until the present. Accordingly, we perform an exhaustive study of the influence of temperature on the static and dynamic properties of polymer melts in search of evidence for the glass transition. The second and most important goal of our work is to study the influence of chain stiffness on T_{g}. We will use bending and torsion potentials to control the chain stiffness, and we will analyze their effect, combined with the temperature, on polymer melt dynamics. Bending stiffness has been used also in (Faller and Müller-Plathe 2001) and (Everaers et al. 2004). In a previous study (Bulacu and Van der Giessen 2005), we analyzed the effect of bending-torsion stiffness on polymer behavior and entanglement at constant temperature $T = 1.0\varepsilon/k_{\mathrm{B}}$. Here we extend our investigation to a large temperature interval $T = (0.05 - 10.0)\varepsilon/k_{\mathrm{B}}$.

From diffusion results, we determine the T_{g} values for three types of chain stiffness and confirm them by investigating the time autocorrelation functions for the dihedral angle and for the end-to-end vector. A comparison is made between results obtained using repulsive versus attractive LJ interactions.

Another contribution of the present chapter is the analysis of the chain length influence on polymer dynamics: how chain length affects the glass transition temperature and how the D versus N dependence is modified by the temperature.

Before presenting and discussing how the static and dynamic melt properties change with temperature, we first briefly review the computational model and the methods used for the generation and equilibration of the polymer systems.

5.2 Model and simulation method

We perform MD simulations of ensembles of entangled polymer chains using a coarse-grained polymer representation based on the Kremer-Grest model (Kremer and Grest 1990). Each chain is constituted by a linear string of beads connected by springs and all the beads interact via a repulsive LJ potential. We have extended this basic model by including bending and torsion potentials to control the chain stiffness and studied their effect on the entanglement length (Bulacu and Van der Giessen 2005). Here we perform an augmented analysis of the combined effects of temperature and chain stiffness.

The simulated systems consist of M chains, each chain containing N beads, and the bead number density is $\rho = 0.85\sigma^{-3}$. The potentials governing the interactions between the beads are given in Table 5.1 and the parameter values used in our simulations are given in Table 5.2. All beads, connected or not, interact through a repulsive Lennard-Jones potential truncated at $r_{\mathrm{c}} = \sqrt[6]{2}\sigma$ (see Eq. (5.4) in Table 5.1). In addition to the LJ

potential, adjacent connected beads also interact through a finite extensible non-linear Elastic (FENE) potential, given in Eq. (5.1). This combination of potentials and parameters prevents the chains from crossing each other during MD and yields entangled ensembles with realistic dynamics for polymer melts (Kremer and Grest 1990).

We control the chain stiffness by using a bending potential V_{B} and a torsion potential V_{T} acting on three and four consecutive connected beads, respectively; see Eqs. (5.2) and (5.3). It is important to note the novelty of the torsion potential V_{T}: it depends not only on the torsion angle ϕ_i, but also on the bending angles θ_{i-1} and θ_i (Bulacu and Van der Giessen 2005). In this way the computational instabilities arising when two successive bonds align are naturally eliminated. We gain the essential advantage that the torsion angles are controlled by an efficient continuous potential, rather than by using computationally expensive rigid constraints. This helps to manage large systems for long simulation time in order to perform diffusion studies.

The dynamics of the polymer chains will always tend to evolve towards the three local minima that correspond to the equilibrium bending angle θ_0 and the three equilibrium states of the dihedral angle ϕ (*trans*, *gauche*$^+$ and *gauche*$^-$) (see Figure 3.6).

While most of our simulations are run using a purely repulsive LJ potential with a cutoff distance $r_{\mathrm{c}} = \sqrt[6]{2}\sigma$, we will also present, for comparison purposes, some results obtained by including also the attractive part with a doubled cutoff distance $r_{\mathrm{c}} = 2\sqrt[6]{2}\sigma$. These two cases will be termed, for simplicity, *LJ repulsive* and *LJ attractive*.

	$V_{\mathrm{FENE}}(r_{ij}) = \begin{cases} -0.5kR_0^2 \ln\left[1-(r_{ij}/R_0)^2\right], r_{ij} \le R_0 \\ \infty\,, r_{ij} > R_0 \end{cases}$ (5.1)
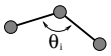	$V_{\mathrm{B}}(\theta_i) = 0.5k_\theta(\cos\theta_i - \cos\theta_0)^2$ (5.2)
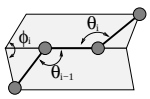	$V_{\mathrm{T}}(\theta_{i-1},\theta_i,\phi_i) = k_\phi \sin^3\theta_{i-1}\sin^3\theta_i \sum_{n=0}^{3} a_n \cos^n\phi_i$ (5.3)
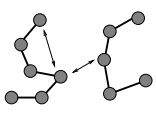	$V_{\mathrm{LJ}}(r_{ij}) = 4\varepsilon\left[\left(\frac{\sigma}{r_{ij}}\right)^{12} - \left(\frac{\sigma}{r_{ij}}\right)^{6} + \frac{1}{4}\right], r_{ij} < r_{\mathrm{c}}$ (5.4)

Table 5.1: *Potentials used in simulations to represent the interactions between beads.*

parameter	in MD units
Lennard-Jones length σ	1
Lennard-Jones minimum energy ε	1
Lennard-Jones cutoff distance r_c	$(2)\sqrt[6]{2}$
FENE elastic constant k	30
Maximum bond elongation R_0	1.5
Bending constant k_θ	25
Bending equilibrium angle $\cos\theta_0$	-0.333
Torsion constant k_ϕ	1
Torsion polynomial coefficients in Eq. (5.3):	
a_0	3.00
a_1	-5.9
a_2	2.06
a_3	10.9

Table 5.2: *Parameters used in simulations.*

The samples for the MD runs are carefully prepared to be compatible with the subsequent simulation conditions. The initial chain conformations are generated in conformity with the type of stiffness that will be induced along the backbone (Bulacu and Van der Giessen 2005):

1. Freely jointed chain (FJC)—intrinsic stiffness only (neither bending nor torsion potentials): initial chains generated as non-reversal random walks;

2. Freely rotating chain (FRC)—bending stiffness (bending potential, no torsion potential): initial chains generated as random walks with fixed bending angle $\theta_0 = 109.5$ deg between consecutive bonds;

3. Rotational isomeric state (RIS)—combined stiffness (both bending and torsion potentials): initial chains generated as random walks with fixed bending angle ($\theta_0 = 109.5$ deg) and fixed dihedral angles $\phi_0 = 60$ deg (*gauche*$^+$, 20% probability), 180 deg (*trans*, 60% probability) and 300 deg (*gauche*$^-$, 20% probability).

After generation, the chains are randomly placed inside the simulation box and then a packing procedure spreads the chains as uniformly as possible using random moves (rotation, translation, reflection), while treating the chains as rigid objects.

A pre-equilibration run follows, employing a capped LJ potential with the aim to eliminate the initial bead overlaps. More details can be found in (Bulacu and Van der Giessen 2005) and (Auhl et al. 2003).

The MD runs are performed at constant volume V and constant temperature T with periodic boundary conditions. The temperature is controlled by coupling the system to a heat bath (Grest and Kremer 1986): the friction coefficient is $\Gamma = 0.5\tau^{-1}$ and the strength of the Gaussian white-noise force is $6k_{\mathrm{B}}T\Gamma$.

The equations of motion are integrated using the 'velocity-Verlet' algorithm (Swope et al. 1982) with a time step related to the temperature values: generally, $\Delta t = 0.01\tau$, but for high temperatures, $\Delta t = 0.006\tau$ or even $\Delta t = 0.003\tau$ has been used.

To extract the static and dynamic properties of the polymer system at a chosen temperature, two types of equilibration procedures were utilized: (i) the systems were generated and equilibrated at that particular temperature or (ii) the systems were cooled in steps from a higher temperature to the desired one by allowing them to equilibrate at each step. We did not find any significant difference between these two techniques (which might be due to our judicious initial generation method).

Results will be presented mainly for systems of $M = 1000$ chains (unless otherwise specified) with different chain length ($N \leq 50$) and stiffness. The simulation of a system with long and stiff polymer chains (RIS) at the lowest temperature required at least 20×10^6 MD steps, or almost 6 weeks of CPU time on a 2.8 GHz/1 GB Pentium 4 processor.

5.3 Results and discussion

Since the glass transition is associated with a dramatic slowing down in the motion of chain segments, we focused our *in silico* study on the temperature dependence of the dynamic properties, with the major goal of finding clear evidence for such internal motion retardation. However, we start out by investigating the static properties not because the glass transition would have a noticeable effect on the long-range static structure, but primarily to prove that the systems are still in the amorphous state even at low temperatures.

5.3.1 Static properties

We consider first the temperature dependence of the characteristic ratio C_N, which is a measure of the spatial extension of the polymer chains, defined as

$$C_N = \left\langle R^2(N) \right\rangle / Nb^2, \tag{5.5}$$

where R is the chain end-to-end distance, N is the number of beads in the chain, and b the mean bond length. Figure 5.1 shows the variation of C_N with the temperature for systems with $M = 1000$ chains of $N = 50$ beads, for the three types of chain stiffness investigated here. The temperature has no significant influence on FJC and FRC chains,

as observed also in other studies (Rigby and Roe 1987, Bennemann et al. 1998). The explanation for this behavior resides in the fact that both the bond (FENE + LJ) and the bending potentials have one energetic minimum. The temperature modifies only the amplitude of the oscillations around this minimum and, as a result, the total effect on C_N is negligible.

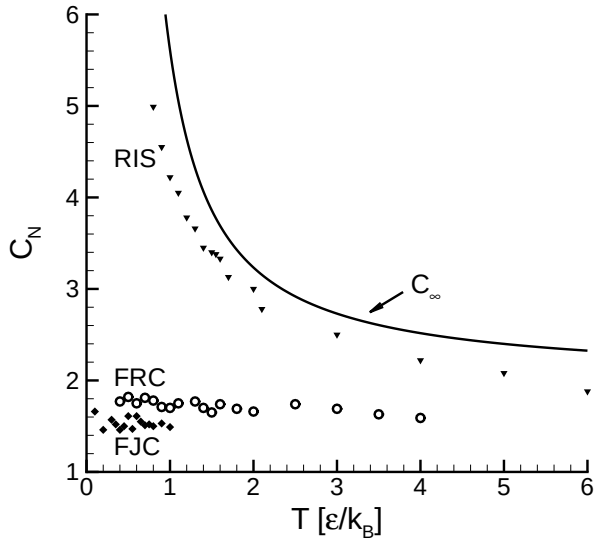

Figure 5.1: *Dependence of the characteristic ratio C_N on the temperature for systems of $M = 1000$ chains with $N = 50$ beads/chain, subjected to intrinsic stiffness (FJC), bending stiffness (FRC) or combined bending-torsion stiffness (RIS). The solid curve is the theoretical prediction for C_∞ versus T (Eq. (5.7)) derived for the classical three-state RIS model (Flory 1969).*

For the RIS case, however, C_N is strongly dependent on temperature. This was previously evidenced by the atomistic simulations of Rigby and Roe (1987), yet their results appeared to have a strong deviation from the theory at low temperatures. Our results from Fig. 5.1 are in good agreement with the theoretical predictions of the classical three-state RIS model (Flory 1969). To illustrate this, let us consider the very simple case of a polymer with a fixed bending angle ($\theta = 109.5$ deg) and three discrete states S allowed for the torsion angle: *gauche*$^+$, *trans* and *gauche*$^-$ ($\phi_S = 60$ deg, 180 deg, 300 deg). The occupancy probability for each state S is given by the Maxwell-Boltzmann distribution

$$p_S = \frac{e^{-V_S/k_\mathrm{B}T}}{Z}, \quad \text{with} \quad Z = \sum_S e^{-V_S/k_\mathrm{B}T}, \tag{5.6}$$

where V_S is V_T from Eq. (5.3) for specific ϕ_S values for each state and for $\theta_i = \theta_{i-1} = 109.5$ deg. The theoretical C_N for infinitely large chains C_∞ is then computed as in (Flory 1969)

$$C_\infty = \frac{1-\cos\theta}{1+\cos\theta}\frac{1-\overline{\cos\phi}}{1+\overline{\cos\phi}}, \quad \overline{\cos\phi} = \sum_{\mathrm{S}} p_{\mathrm{S}} \cos\phi_S, \tag{5.7}$$

and its dependence on T is drawn as the solid curve in Fig. 5.1. It is notable that this theoretical inference reproduces qualitatively very well the experimental results for the entire temperature interval considered in the MD simulations. The difference between the predicted curve and the experimental data points can be explained on the basis of the disparity in complexity between the simulated systems and the presented theoretical model. Three opposing effects play a major role, altering C_∞ according to Eq. (5.7): (1) in the simulated systems the chain length is finite ($N = 50$); (2) while the initial configurations of the polymers are generated with fixed torsion angles corresponding to the discrete states *gauche*$^+$ (20%), *trans* (60%) and *gauche*$^-$ (20%), later during MD the torsion angles take continuous values, because the torsion potential itself is continuous; (3) the torsion potential V_{T} influences the equilibrium bending angle θ_0 and pushes the distribution of bending angles towards larger values.

Nevertheless, the three-state RIS model captures the temperature influence very well: as temperature increases, the probability for *trans* state decreases, while the probabilities for the intermediate torsion angles increase, thus naturally leading to shorter chains, as observed in simulation. For very high temperatures, all dihedral angles become equally probable and C_N tends to the value of the FRC case. This asymptotic behavior at high temperatures can indeed be observed in Fig. 5.1. At the opposite end, towards low temperatures, the increase in C_N with decreasing temperature continues without any sign of cessation of the *trans-gauche* conformational transitions. Our results disagree with the observations reported by Rigby and Roe (1987), who measured an almost constant C_N below a certain temperature, contrary to the theory.

We have also investigated the pair-distance correlation function $g(r)$, given in Fig. 5.2, in order to see how the temperature affects the local structure of the polymer melt. It is important to observe from the beginning that the peaks present in the calculated pair-distance functions are due exclusively to the bonds along the chain backbone and to the LJ coordination shells. There are no intermediary peaks that would have signaled the presence of crystallization. The first sharp peak represents the cumulated contributions of the polymer bonds ($b = 0.96\sigma$) and the first LJ shell ($r_{\mathrm{c}} = \sqrt[6]{2}\sigma \approx 1.122\sigma$). At high temperatures, these distances merge to become a collective peak around $r \approx \sigma$. Upon cooling, this peak splits more and more evidently into two separate peaks, as observed also in (Bennemann et al. 1998). The dashed curves in Fig. 5.2 (FJC) were obtained by including also the attractive part of the LJ potential ($r_{\mathrm{c}} = 2\sqrt[6]{2}\sigma$): for decreasing temperature, the peak due to the first LJ shell surpasses the peak due to the bonds and the remaining LJ peaks become more evident. The second LJ coordination shell is visible in a peak at $\approx 2.2\sigma$.

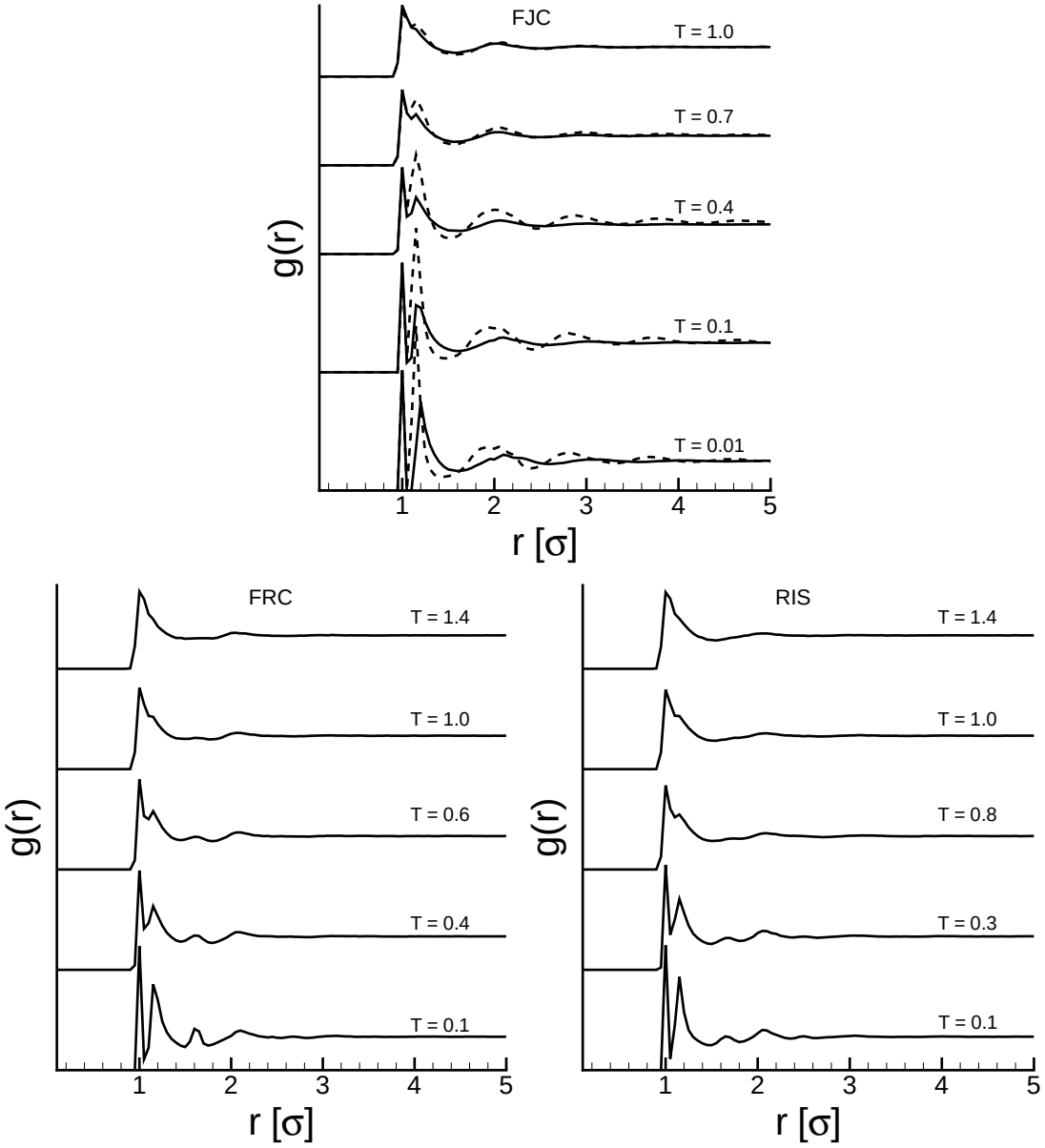

Figure 5.2: *Pair-distance correlation function $g(r)$ at different temperatures (in MD units) for the three types of chain stiffness. All systems contain $M = 1000$ chains, $N = 50$ beads/chain. The dashed lines correspond to LJ attractive case for FJC chains. The curves for higher temperatures are shifted upward for better visualization.*

The bending potential in FRC chains induces an additional peak at $\approx 1.6\sigma$ (see Fig. 5.2, FRC). This peak is more distinct at low temperatures and for higher values of the bending constant k_θ. This bending peak is attenuated for RIS chains, because the torsion potential tends to straighten the bending angles.

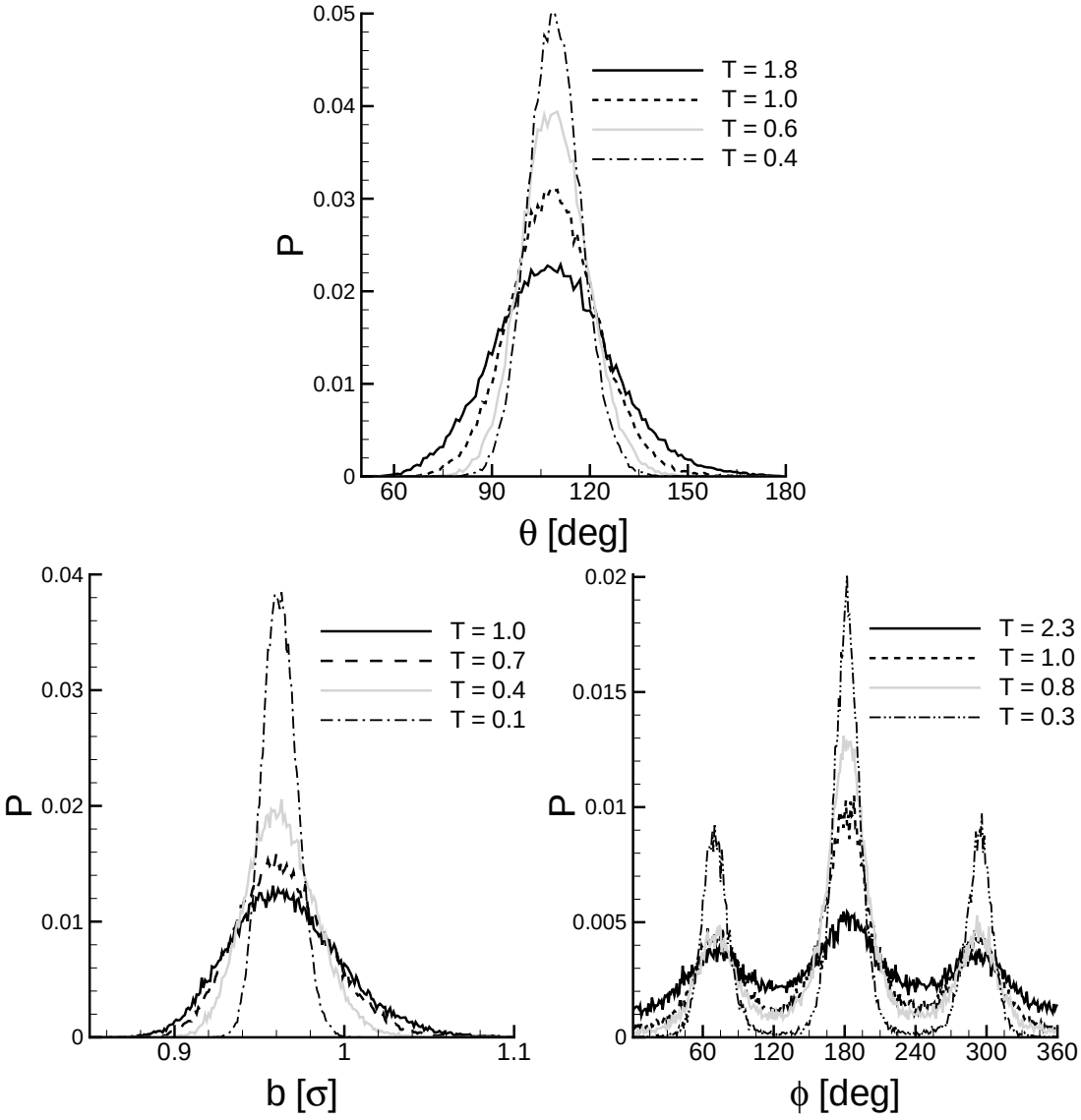

Figure 5.3: *Histograms of bond lengths b ($k = 30$, $k_\theta = 0$ and $k_\phi = 0$), bending angles θ ($k = 30$, $k_\theta = 25$ and $k_\phi = 0$) and torsion angles ϕ ($k = 30$, $k_\theta = 25$ and $k_\phi = 1$) at different temperatures ($M = 1000$ chains, $N = 50$ beads/chain).*

The direct effect of the potentials controlling the chain stiffness can be clearly observed in the histograms of the bond lengths, bending angles, and torsion angles. For FJC and FRC chains, lower temperatures result in higher and sharper peaks around the equilibrium bond length and bending angle (see Fig. 5.3). For high temperatures, when the distributions are broad, an asymmetry can be observed with respect to the maximum: this is the expression of the asymmetry of the underlying potentials acting on the bonds (FENE + LJ) and on the bending angles (V_B). For RIS chains, the probability

of intermediate torsion angles increases with increasing temperature, at the expense of the *trans*, *gauche*$^+$ and *gauche*$^-$ states. All values for the torsion angles tend to become equiprobable and this leads to more coiled chains with lower characteristic ratio C_N (fact already noticed above).

5.3.2 Dynamic properties

In this sub-section we analyze how the temperature influences the polymer chain dynamics by studying the chain self-diffusion and the time decay of the autocorrelation functions for torsion angle and for end-to-end distance.

Diffusion strongly depends on the temperature that directly affects the accessible free volume, the chain stiffness and the type of chain motion inside the polymer bulk. According to the Rouse model (Rouse 1953), the diffusion coefficient D depends on temperature and chain length as

$$D_{\mathrm{Rouse}} = \frac{k_{\mathrm{B}}T}{\zeta N}, \tag{5.8}$$

with ζ the effective bead friction coefficient. For long entangled chains, reptation theory (de Gennes 1979, Doi and Edwards 1989) predicts a different formula for D, implying a drastic slowing down of chain motion:

$$D_{\mathrm{reptation}} = \frac{1}{3}\frac{d_{\mathrm{T}}^2}{l^2}\frac{k_{\mathrm{B}}T}{\zeta N^2}, \tag{5.9}$$

where d_{T} is the reptation tube diameter and l is the effective bond length. Both Eqs. (5.8) and (5.9) include an explicit linear T-dependence as well as an implicit one via the friction coefficient ζ or the reptation tube diameter d_{T}. The dependence on T of these parameters has not been predicted on pure theoretical grounds and remains to be determined empirically by physical experiments and computer simulations.

The self-diffusion coefficient D, characterizing the macroscopic transport of the chains inside the polymer melt, is calculated from the mean-square displacement $g_3(t)$ of the chain center of mass $\mathbf{r}_{\mathrm{CM}}$

$$g_3(t) = \frac{1}{M}\left\langle |\mathbf{r}_{\mathrm{CM}}(t) - \mathbf{r}_{\mathrm{CM}}(0)|^2 \right\rangle , \tag{5.10}$$

using the Einstein relation

$$D = \lim_{t\to\infty} \frac{1}{6t} g_3(t) . \tag{5.11}$$

A proper value for D can only be obtained from MD simulations after the chains have diffused over distances larger than their radius of gyration. We have ensured that

the computing times were long enough for this condition to be met even for the longest stiff chains and for the lowest temperatures. During the MD runs the center of mass of the whole melt was held fixed to eliminate its drift due to the stochastic force that models the thermostat.

Let us first consider the behavior of g_3 as a function of time for a relatively short time interval at the beginning of the diffusion process. Figure 5.4 presents results for g_3 corresponding to all three types of chain stiffness studied at different temperatures in a short-time window early in the simulation. For all three cases, $g_3(t)$ shows two clear regimes: one at very short times (when g_3 grows approximatively as t^2) and one at very long times (when $g_3 \propto t^1$, allowing the actual calculation of the limit value for D). Between these two extremes, for rather low temperatures, a third transitional regime appears as an intermediary plateaulike region for FRC and RIS chains. This type of effect, considered a sign of the glass transition, was observed previously in computer simulations using other polymer models (Roe 1994, Bennemann et al. 1998, Tsige and Taylor 2002). However, when one inspects the graphs in Fig. 5.4, the estimation of the glass transition temperature from this effect seems daring, to say the least. The intermediary plateaulike regime caused by decreasing temperature does not appear for the FJC chains when only the repulsive part of the LJ is considered. However, when the calculations are repeated for the LJ attractive case we do observe this effect (results not shown here), as reported previously by Bennemann et al. (1998).

The main results of our simulation work are presented in Fig. 5.5, showing the temperature dependence of D, for all three types of chain stiffness. At each temperature, the values of D were obtained in two ways: (a) generating and equilibrating the system at the desired temperature (full symbols); and (b) generating the system at a higher temperature and then cooling it down in steps and equilibrating until the desired temperature is reached (open symbols). Within statistical fluctuations, these two techniques yield the same results.

In Fig. 5.5, the dependence of the diffusion coefficient D as a function of the temperature T follows an expected behavior: higher temperatures lead to higher diffusion coefficients. This qualitative trend is independent of chain stiffness. The essential feature captured in the present results is that, for sufficiently low temperatures, diffusion coefficient seems to vanish as the polymeric systems freeze into the glassy state. The glass transition temperature T_{g} is estimated by extrapolating $D(T)$ to $D = 0$ —i.e., an apparent cessation of diffusion with respect to the observation time. The resulting values of T_{g} for the three types of polymer chains under consideration are given in Table 5.3. The systems are not likely to undergo a sharp transition at these temperatures that should be considered as a estimate of the temperature interval associated with the glass transition. We are more interested in the stiffness effects on the glass transition than in very accurate values for T_{g} itself.

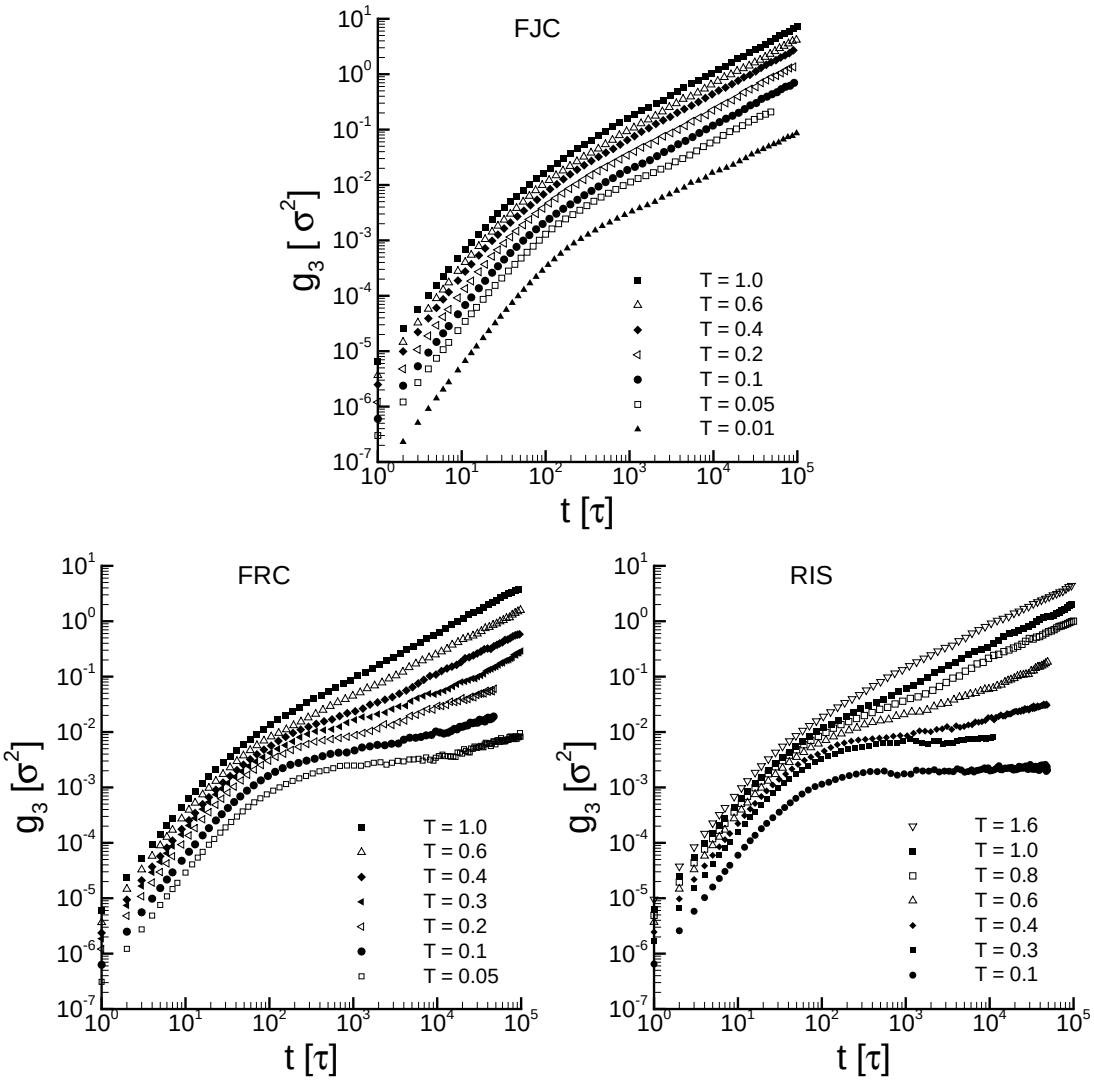

Figure 5.4: *Close-up view in the short relaxation time region of the time dependence of the mean-square displacement of the chain center of mass (g_3). For all three stiffness cases the temperatures are indicated in the insert. Only a relatively short time interval, at the beginning of the simulations, is depicted to distinguish more clearly the plateaulike intermediary regime that appears at lower temperatures for FRC and RIS chains.*

Another possible way to estimate T_g would be the fitting of D vs. T curves with different empirical or theoretical equations (Jäckle 1986, Götze and Sjögren 1992) that provides an inferior limit for T_g. Since the results are very much dependent on the temperature interval used for the fitting and since we consider that the MD simulations are not accurate enough to distinguish between exponentially small and strictly zero values of the diffusion coefficients close to the glass transition temperature, we do not

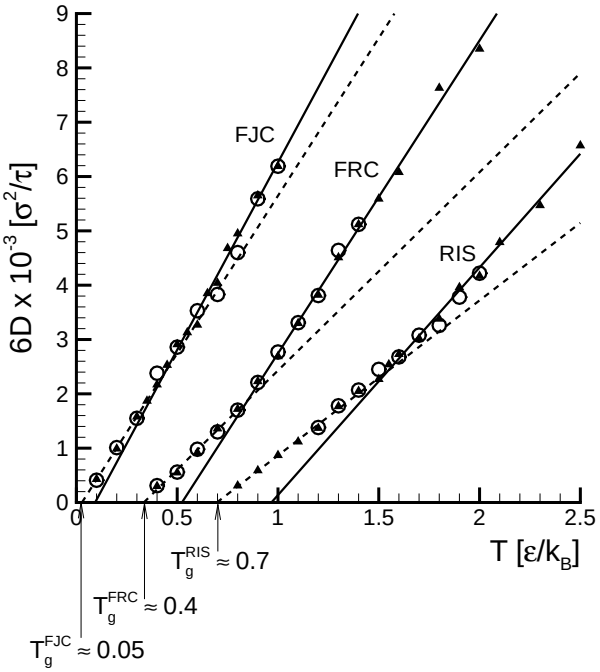

Figure 5.5: *Temperature dependence of the self-diffusion coefficient D for systems with $M = 1000$ chains, $N = 50$ beads/chain, with FJC, FRC and RIS stiffness. Solid symbols are obtained from simulations at the indicated temperatures and open symbols are obtained after cooling from higher temperatures to the desired temperatures. The solid symbols are used to define two linear regimes (the straight lines drawn in the figure).*

	T_{g} $[\varepsilon/k_{\mathrm{B}}]$
FJC ($k_\theta = 0$, $k_\phi = 0$)	0.05
FRC ($k_\theta = 25\varepsilon$, $k_\phi = 0$)	0.4
RIS ($k_\theta = 25\varepsilon$, $k_\phi = 1\varepsilon$)	0.7

Table 5.3: *Estimated values of the glass transition temperature T_{g} for the three types of chain stiffness FJC, FRC and RIS. These approximate T_{g} values are consistent with the diffusion results shown in Fig. 5.5 and with the relaxation times shown in Fig. 5.11.*

perform such a fitting.

It is important to observe that T_{g} increases with polymer stiffness from FJC to FRC, and further to RIS chains, by controlling the elastic constants of the bending (k_θ) and torsion (k_ϕ) potentials. This is consistent with the observation that, at a given temperature, D decreases when the chain stiffness increases (a result already reported in our previous paper (Bulacu and Van der Giessen 2005) for $T = 1\varepsilon/k_{\mathrm{B}}$).

The D vs. T graphs in Fig. 5.5 show two linear regimes with different slopes: a fast regime specific to the liquid (melt) phase and a slower regime corresponding to supercooled and highly viscous systems situated between the glassy and the liquid states. The crossover temperature T_c between these two regimes increases also with increasing stiffness: $T_c \approx 0.4\varepsilon/k_B$ for FJC, $T_c \approx 0.8\varepsilon/k_B$ for FRC and $T_c \approx 1.5\varepsilon/k_B$ for RIS.

An essential element influencing the polymer dynamics is whether the LJ potential is purely repulsive ($r_c = \sqrt[6]{2}\sigma$) or includes also an attractive part ($r_c = 2\sqrt[6]{2}\sigma$). For comparing with the work of Bennemann et al. (1998) where an attractive LJ potential was used for systems with FJC chains ($N = 10$ beads/chain), we have also simulated identical systems for both values of the LJ cutoff distance r_c. The resulting $D(T)$ for FJC systems shown in Fig. 5.6 agree very well with the results in (Bennemann et al. 1998). We observe that for temperatures below $T = 1.0\varepsilon/k_B$, the diffusion coefficients are significantly smaller when the attractive LJ interaction is considered. Above this temperature, there is no difference in the diffusion coefficients, as stated previously by Kremer and Grest (1990). The reduced diffusion for an attractive LJ interaction can be explained by observing that the second LJ coordination shell falls within the attractive region of the potential. This will reduce the motion of the beads of the first LJ coordination shell, thus diminishing the overall diffusion. Consequently, the glass transition temperature for systems with attractive LJ ($T_g \approx 0.4\varepsilon/k_B$) is considerably higher than for systems with only repulsive LJ.

The effectiveness of the bead mobility in controlling the glass transition depends not only on temperature and chain stiffness but also on the chain length N. T_g increases with the chain length to a plateau value T_g^∞, specific to infinitely long polymer chains following a universal relation well established in the literature (Fox and Flory 1950, Rudin and Burgin 1975):

$$T_g N = T_g^\infty (N - \text{const}), \tag{5.12}$$

where the constant depends on the particular polymer type. Figure 5.8 shows our results for the chain length dependence ($N \leq 50$) of T_g for FRC and RIS chains and Figure 5.7 shows D vs. T dependences at different chain lengths from which the glass transition temperature was obtained.

T_g^∞ and the constant from Eq. (5.12) are estimated by linearly fitting the $T_g N$ vs. N dependence and the resulting curves are included in Fig. 5.8. This is an elegant method to estimate T_g values for systems of long polymer chains, avoiding otherwise extremely time-consuming simulations. The specific T_g^∞ values ($\approx 0.47\varepsilon/k_B$ for FRC and $\approx 0.75\varepsilon/k_B$ for RIS) are very close to T_g for $N = 50$ beads per chain, indicating this considered length as a good choice to compromise between accuracy and computing time.

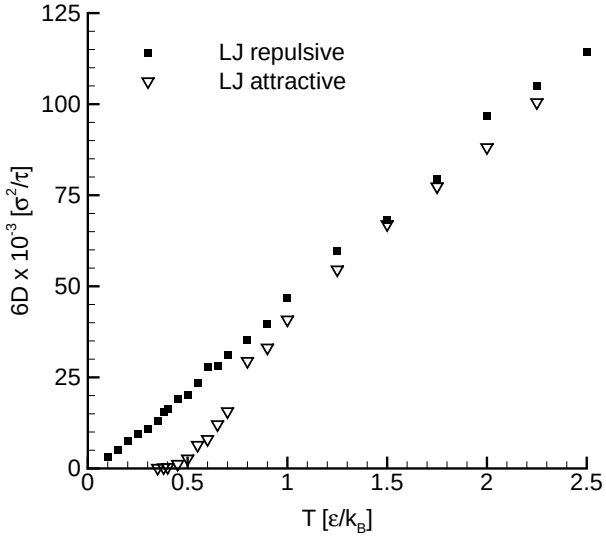

Figure 5.6: *Temperature dependence of the self-diffusion coefficient D for systems with $M = 1000$ chains, $N = 10$ beads/chain, with FJC (intrinsic) stiffness. Solid symbols are obtained from simulations with repulsive LJ potential ($r_c = \sqrt[6]{2}\sigma$) and open symbols are obtained for attractive LJ potential ($r_c = 2\sqrt[6]{2}\sigma$). The glass transition temperature for the attractive LJ case is $T_g \approx 0.4$, as reported earlier in (Bennemann et al. 1998).*

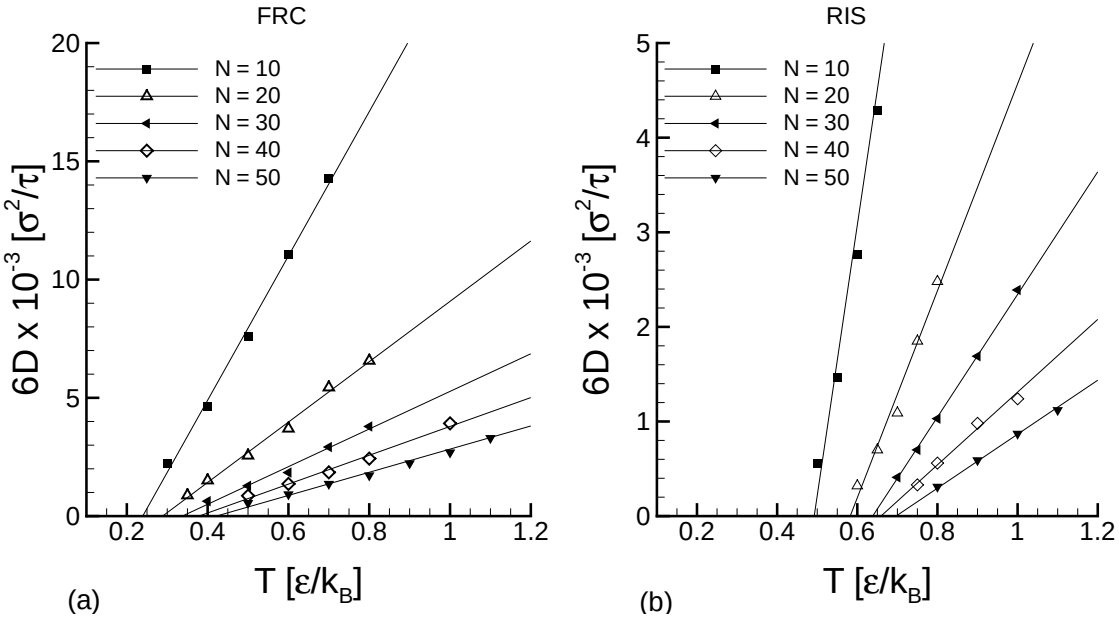

Figure 5.7: *The chain length effects on D vs. T dependences for FRC (a) and RIS chains (b). The lines are linear fits of the symbols.*

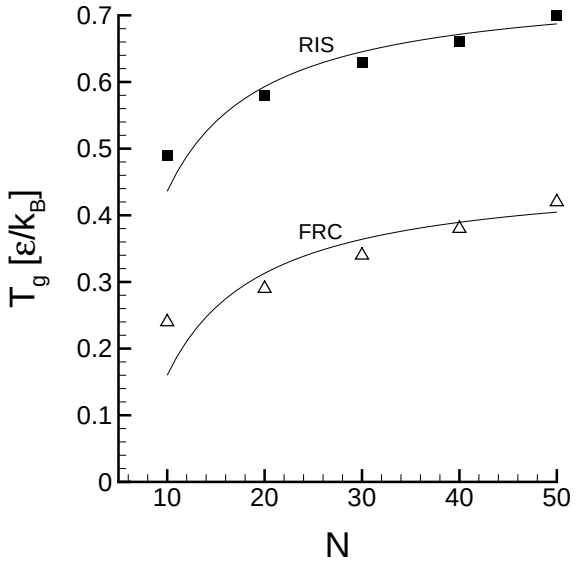

Figure 5.8: *The chain length effects on the glass transition temperature. The curves represent the fitting with Eq. (5.12).*

The chain length dependence of the diffusion coefficient is, in turn, strongly influenced by stiffness and temperature. We show now in Fig. 5.9 the dependence of D on N for temperatures ranging, for each type of stiffness, from the vicinity of $T_{\rm g}$ to well above $T_{\rm c}$—i.e., in the full liquid phase.

Due to the excessive computational time required by simulations at low temperatures and high stiffness for rather large systems of $M = 1000$ chains needed for stable statistical results, we had to limit our study to short chains $N \leq 50$ for which Rouse behavior is expected; i.e. $D \propto N^{-\nu}$ with $\nu = 1$ in concordance with Eq. (5.8).

Similar to prior work in this field (Kremer and Grest 1990, Faller and Müller-Plathe 2001, Bulacu and Van der Giessen 2005), rather than D vs. N, we plot $6DN$ vs. N in logarithmic scales since this allows for an easy distinction between the horizontal plateau of the Rouse regime and the slanted dependence ($\nu > 1$) characteristic for reptation.

At relatively high temperatures, above $T_{\rm c}$, the chains behave according to the Rouse theory for all three types of chain stiffness. However, with increasing stiffness, higher temperatures are needed to obtain the nearly horizontal dependence. A noteworthy observation from Fig. 5.9 is that, for FRC and RIS chains, at temperatures approaching $T_{\rm g}$, the DN vs. N dependence becomes progressively inclined, thus testifying to the dissolution of the Rouse regime for super-cooled polymer melts.

For each temperature, the data in Fig. 5.9 have been fitted to $D \propto N^{-\nu}$; the values of the exponent ν for the three types of chain stiffness are gathered in Table 5.4.

Our results for the temperature effects on the D versus N dependence can be put

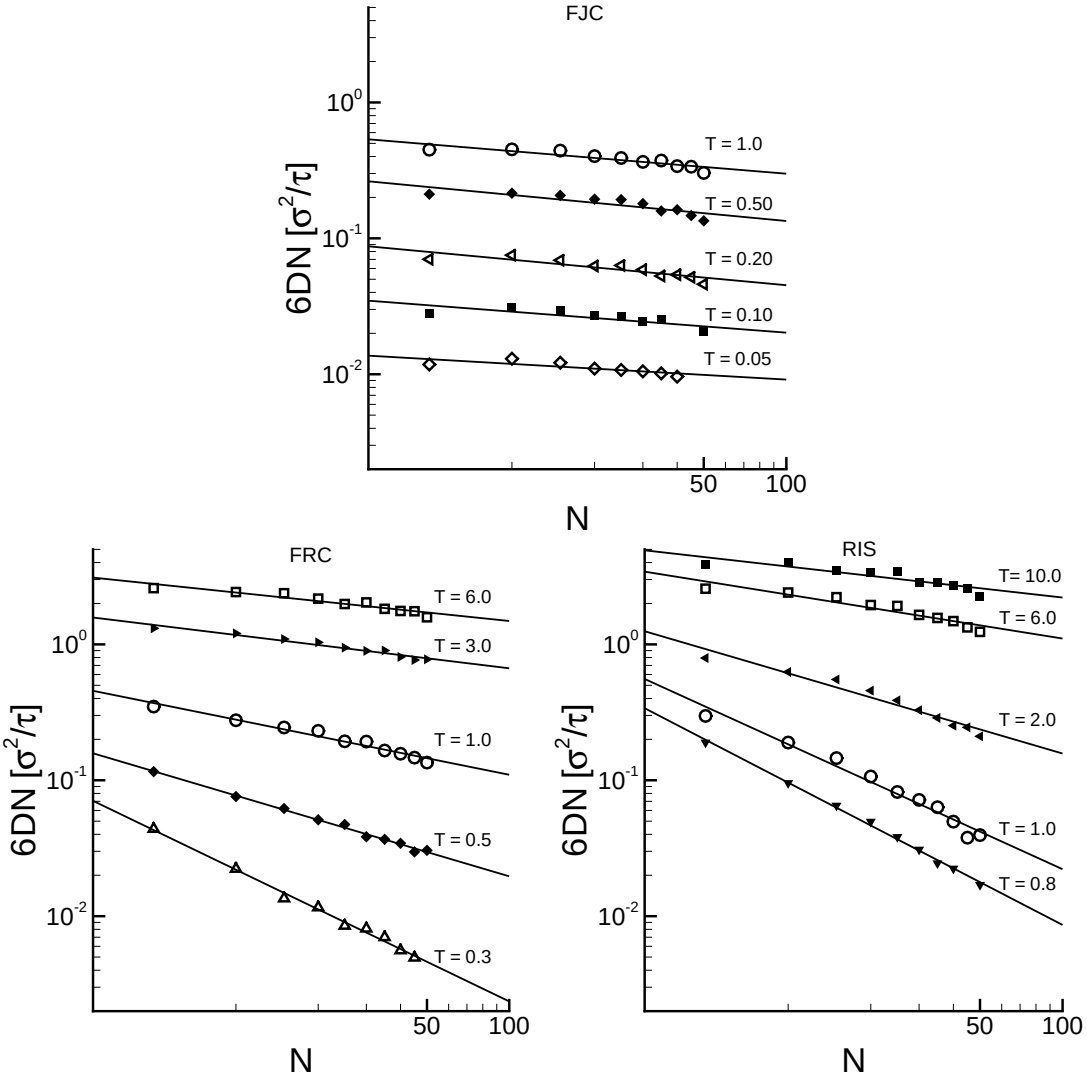

Figure 5.9: *Self-diffusion coefficient D for FJC, FRC and RIS chains as a function of chain length N at different temperatures (simulated systems with $M = 1000$ chains). The temperatures are indicated in each figure in MD units. The dependence becomes progressively inclined as the temperature is lowered approaching T_{g}.*

in a more general theoretical and experimental context. A modified free-volume theory has been proposed by von Meerwall et al. (1982, 1998) that combines the Rouse theory with free-volume effects due to the chain ends. This combined Rouse-free-volume theory predicts a gradual change of the exponent ν in $D \propto N^{-\nu}$ with temperature, which has been tested experimentally (von Meerwall et al. 1998) and in atomistic simulations (Harmandaris et al. 2002) for n-alkanes. Our results agree qualitatively with these previous studies when the coarse-grained model is augmented with additional bending and

FJC		FRC		RIS	
$T\ [\varepsilon/k_\mathrm{B}]$	ν	$T\ [\varepsilon/k_\mathrm{B}]$	ν	$T\ [\varepsilon/k_\mathrm{B}]$	ν
0.05	1.12	0.3	1.97	0.8	2.00
0.10	1.16	0.5	1.59	1.0	1.92
0.20	1.19	1.0	1.41	1.5	1.65
0.50	1.19	1.5	1.33	2.0	1.59
1.00	1.17	3.0	1.25	6.0	1.32
1.50	1.17	6.0	1.21	10.0	1.23

Table 5.4: *Influence of the chain stiffness and temperature on the exponent ν in the power law $D \propto N^{-\nu}$. The exponents have been calculated by fitting the data from Fig. 5.9.*

torsion stiffness.

We find further evidence of the glass transition by investigating the time autocorrelation functions (ACFs) of the torsion angle and of the end-to-end vector.

The torsion angle autocorrelation function R_ϕ has the fastest relaxation time, and we expect to reflect the dramatic slowing down of the local chain dynamics induced by the glass transition. For its calculation, we preferred to use Eq. (5.13) (proposed in (Takeuchi and Okazaki 1990)) because this formulation uses cosine functions and avoids the expensive computation of the actual values of the dihedral angles:

$$R_\phi(t) = \frac{\langle \cos\phi_i(t)\ \cos\phi_i(0)\rangle - \langle \cos\phi_i(0)\rangle^2}{\langle \cos\phi_i(0)\ \cos\phi_i(0)\rangle - \langle \cos\phi_i(0)\rangle^2}, \tag{5.13}$$

where $\phi_i(t)$ is a dihedral angle at time t and the averages are calculated over all dihedrals in the system and over several time references. The $R_\phi(t)$ plots in Fig. 5.10 reveal the same trend for all three stiffness: as the temperature decreases, R_ϕ relaxes more slowly, to the limit of almost no relaxation at very low temperatures during the observation time.

The relaxation time τ_R specific for each situation was estimated as the time at which R_ϕ has decayed to $1/e$ from its initial value. In this way we deliberately avoid employing any theoretical or empirical models since there is no clear evidence that they are appropriate to both below and above T_g regimes (Jin and Boyd 1998). The temperature dependence of the relaxation time τ_R is shown in Fig. 5.11 (solid symbols, left scale).

The calculated relaxation time for the torsion autocorrelation function increases monotonically with decreasing temperature until a specific temperature is reached. At this temperature a sudden increase of the relaxation time occurs, indicating a strong slowing down of the torsion dynamics. By identify this temperature with the glass transition temperature, we obtain, for all chain types, very similar T_g values with the one obtained from the vanishing of the diffusion coefficient D; cf. Fig. 5.5.

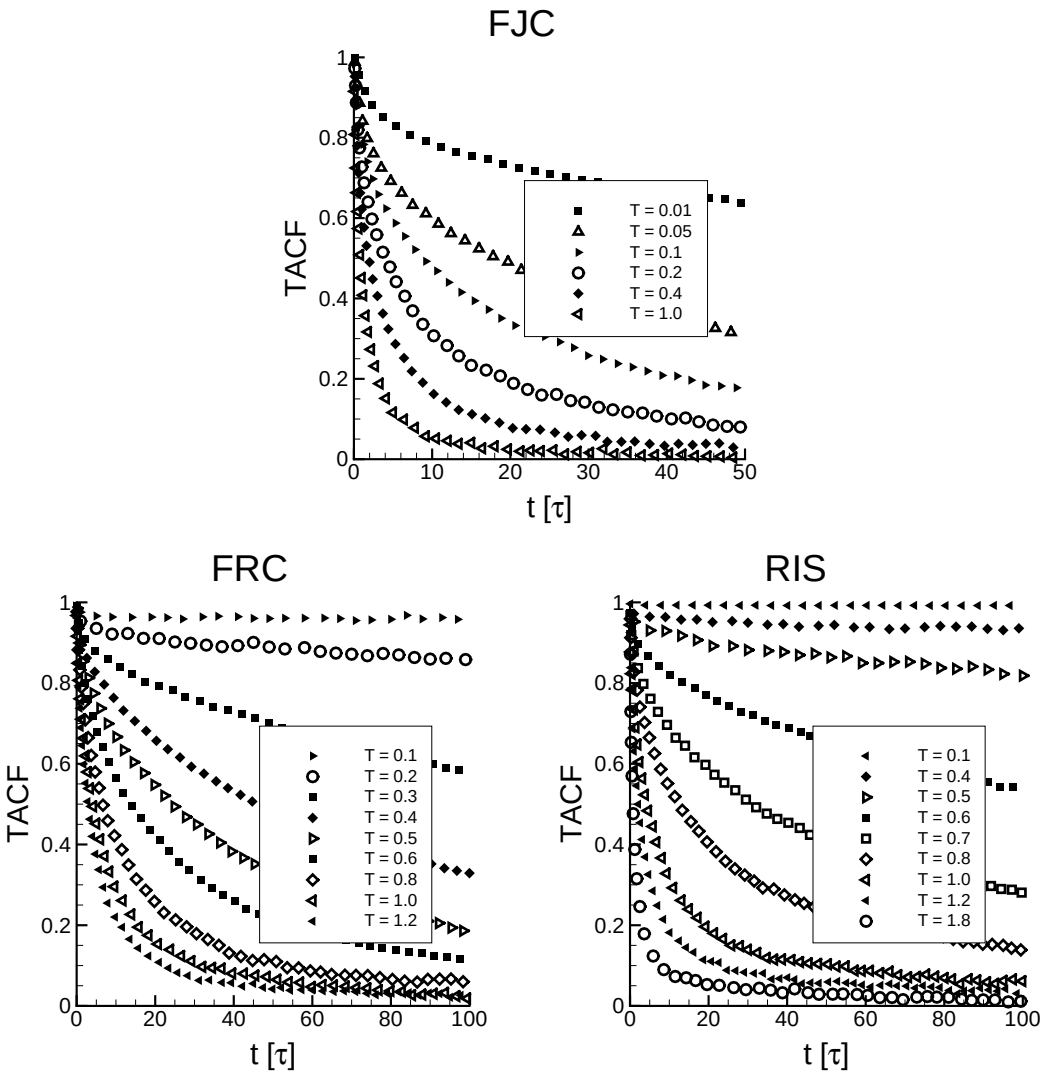

Figure 5.10: *The decay in time of the torsion angle autocorrelation function R_ϕ at various temperatures for FJC, FRC and RIS chains. The temperatures are indicated in the insert in $\varepsilon/k_{\mathrm{B}}$ ($M = 1000$ chains with $N = 50$ beads/chain).*

We have also investigated the time autocorrelation function of the end-to-end vector $\langle \mathbf{R}(t) \cdot \mathbf{R}(0) \rangle \,/\, \langle R^2(0) \rangle$. The relaxation times τ_{E}, computed as described above, are given in Fig. 5.11 (open symbols, right scale). We observe a remarkable resemblance of the results, indicating almost the same T_{g} values, even though time scales of these two processes are completely different. The autocorrelation function of the end-to-end vector has the slowest relaxation time that is needed for the end-to-end vector to lose the memory of its initial orientation.

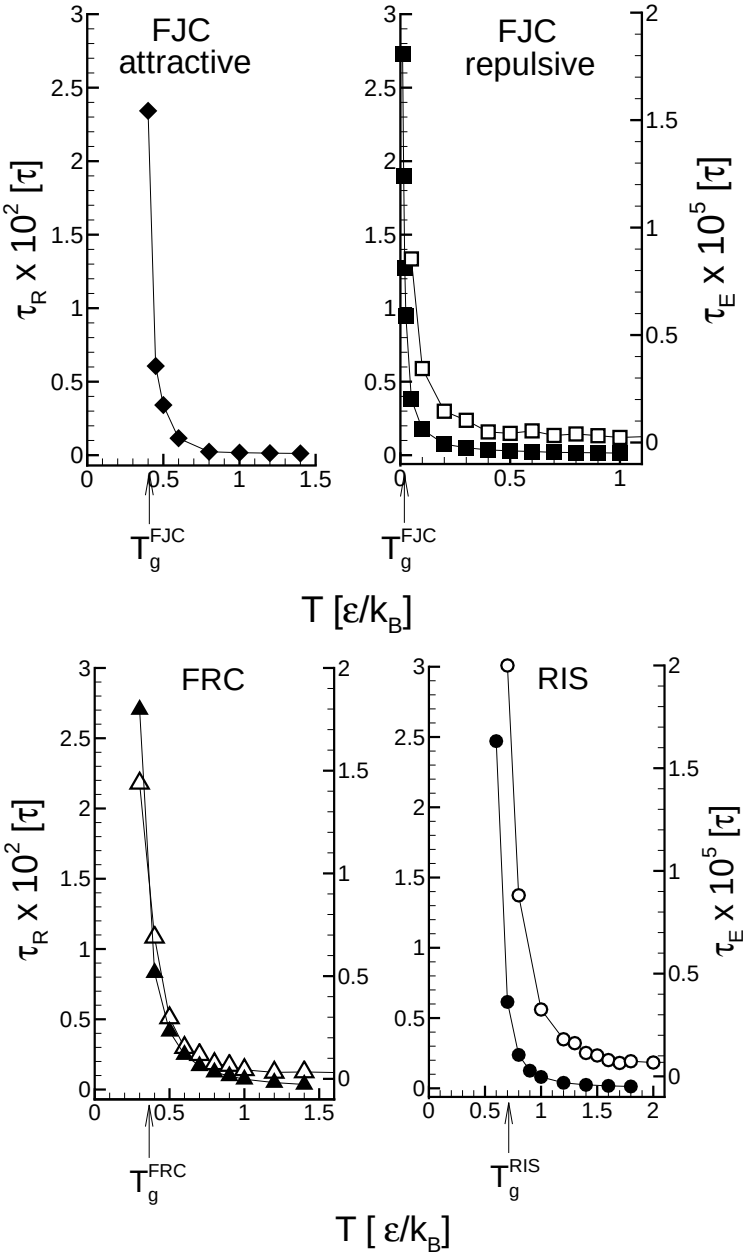

Figure 5.11: *Relaxation time τ_{R} of the torsion autocorrelation function (solid symbols, left scale) and relaxation time τ_{E} of the end-to-end vector autocorrelation function (open symbols, right scale). The relaxation times increase markedly when the temperature is lowered towards T_{g} ($M = 1000$ chains with $N = 10$ beads/chain for attractive FJC and $M = 1000$ chains with $N = 50$ beads/chain for repulsive FJC, FRC and RIS).*

5.4 Conclusions

We have presented comprehensive results from extensive molecular dynamics simulations of ensembles of polymer chains. The computations are based on a coarse-grained chain representation, in the spirit of the Kremer-Grest model, but with additional bending and torsion potentials to control the chain stiffness. Our study covered a large temperature interval and we focused our analysis on the behavior of the polymer systems undergoing glass transition as the temperature is lowered.

First, the static properties of the systems were investigated as a function of temperature. We found that the characteristic ratio is strongly dependent on temperature for RIS chains: the simulation results are in good agreement with the theoretical three-state model, proving the suitability and effectiveness of our novel combined potential that controls the bending and torsion angles. The peaks in the pair-distance distributions corresponding to the LJ coordination shells were used to verify that the polymer ensemble remains in an amorphous state at the lowest temperatures studied. Histogram analysis showed that, by decreasing the temperature, the distributions of bond lengths, bending angles and torsion angles become more narrow around the equilibrium values due to the retardation of the bead mobility.

The most important aspect treated here is the effect of temperature and chain stiffness on the polymer dynamics monitored through the chain self-diffusion coefficient D. For the three type of stiffness considered—FJC, FRS and RIS—the D versus T curves were used to identify the glass transition temperature $T_{\rm g}$ as the limiting value where diffusion vanishes. By increasing the stiffness from FJC to FRC and to RIS chains, the calculated value of $T_{\rm g}$ increases. Investigation of the time autocorrelation functions of the end-to-end vector and of the dihedral angle provided further evidence regarding the glass transition. The relaxation times of these autocorrelation functions show a dramatic increase near the $T_{\rm g}$ estimates obtained from diffusion. This confirmation is significant because the time scales involved differ by about three orders of magnitude. While most of our simulations were run using a purely repulsive LJ potential, some additional comparisons with previous studies were performed by including also the attractive part of the LJ potential. The attractive LJ interactions change the polymer dynamics at low temperatures so as to increase the value of $T_{\rm g}$.

We also provided here a relevant study regarding how the temperature affects the D versus N dependence for relatively short chains: with decreasing the temperature, the exponent in $D \propto N^{-\nu}$ increases from $\nu \approx 1$ (as expected for short chains in Rouse regime) to $\nu \approx 2$. This "fanning out" of the DN vs. N curves at different temperatures, depicted schematically in Fig. 5.12, is stronger for systems with added bending and/or torsion stiffness along the polymer backbone.

Overall, our results indicate that the continuum coarse-grained model employed in

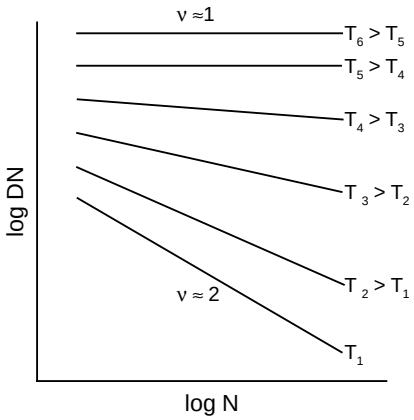

Figure 5.12: *Schematic representation of DN vs. N dependences at different temperatures, for FRC and RIS stiffness. ν is the exponent in $D \propto N^{-\nu}$. The curves "fan out" from $\nu = 1$ to $\nu = 2$ as the temperature decreases towards T_{g}.*

our MD simulations can be very effectively used to study how the microscopic bead motion controlled by the temperature thermostat results in the macroscopic transport process of chain diffusion. The glass transition occurs at temperatures low enough such that the local random bead motion becomes ineffective in inducing large-scale chain diffusion. This phenomenon was distinctly captured in our MD results. The chain flexibility plays a dominant role in polymer dynamics and glass transition, clearly influencing the sensitivity of chain mobility to temperature.